

# **Click Synthesized Dianthryl-TTFV as Highly Sensitive Fluorescent Turn-On Sensor for Cu<sup>2+</sup>, Fe<sup>2+</sup> and Cd<sup>2+</sup> Ions**

*Karimulla Mulla, Prateek Dongare, David W. Thompson, and Yuming Zhao\**

Department of Chemistry, Memorial University of Newfoundland  
St. John's, Newfoundland A1B 3X7, Canada

*Email: yuming@mun.ca*

## **Table of Contents**

1. Experimental	S 2
2. NMR Spectroscopic Data	S 4
3. UV-Vis and Fluorescence Spectral Data	S 12
4. Cyclic Voltammetric Data	S 28

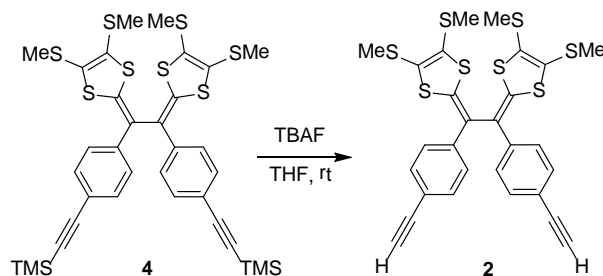
## 1. Experimental

### 1.1 General

Chemicals were purchased from commercial suppliers and used directly without purification. All reactions were conducted in standard, dry glassware and under an inert atmosphere of nitrogen unless otherwise noted. Evaporation and concentration were carried out with a water-aspirator. Flash column chromatography was performed using 240-400 mesh silica gel, and thin-layer chromatography (TLC) was carried out with silica gel F254 covered on plastic sheets and visualized by UV light. Melting points (m.p) were measured with Fisher-Jones melting point apparatus and are uncorrected.  $^1\text{H}$  and  $^{13}\text{C}$  NMR spectra were measured on a Bruker Avance 500 MHz spectrometer. Chemical shifts are reported in ppm downfield from the signal of the internal reference  $\text{SiMe}_4$  for  $^1\text{H}$  and  $^{13}\text{C}$  NMR spectra. Coupling constants ( $J$ ) are given in Hz. Infrared spectra (IR) were recorded on a Bruker tensor 27 spectrometer. MALDI-TOF MS analyses were performed on an Applied Biosystems Voyager instrument using dithranol as the matrix. TTFV precursor **4**<sup>1</sup> and azido anthracene **3**<sup>2</sup> were prepared according to the literature procedures.

### 1.2 Synthesis

#### TTFV diyne **2**

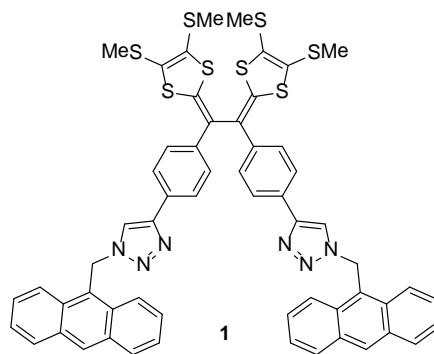


To a solution of compound **4** (350 mg, 0.46 mmol) in THF (5 mL) was added  $\text{Bu}_4\text{NF}$  (60.2 mg, 0.23 mmol) under  $\text{N}_2$ . The resulting yellow solution was stirred for 20 min at rt. After the reaction mixture was completed as checked by TLC analysis, the solvent was removed under reduced pressure. The residue was diluted with  $\text{CH}_2\text{Cl}_2$ , washed with water, dried over  $\text{MgSO}_4$ , and concentrated under reduced pressure. The resulting solid mass was rinsed with methanol (5 mL) to give pure compound **2** (246 mg, 0.40 mmol, 87%) as yellow solid. m.p. 140.1-142.3 °C; IR (neat) 3276, 2916, 2096, 1595, 1471, 1309, 885, 833  $\text{cm}^{-1}$ ;  $^1\text{H}$  NMR (500 MHz,  $\text{CDCl}_3$ ):  $\delta$  7.43 (d,  $J$  = 8.4 Hz, 4H), 7.35 (d,  $J$  = 8.4 Hz, 4H), 3.08 (s, 2H), 2.43 (s, 6H), 2.39 (s, 6H);  $^{13}\text{C}$  NMR (125 MHz,  $\text{CDCl}_3$ ):  $\delta$  138.3, 137.2, 132.5, 128.6, 126.3, 125.2, 123.3, 120.1, 83.6, 77.8, 18.9, 18.8; HRMS (MALDI-TOF, +eV)  $m/z$  calcd for  $\text{C}_{28}\text{H}_{22}\text{S}_8$  613.9487, found 613.9497  $[\text{M}]^+$ .

(1) Chen, G.; Mahmud, I.; Dawe, L. N.; Daniels, L. M.; Zhao, Y. *J. Org. Chem.* **2011**, 76, 2701-2715.

(2) Varazo, K.; Xie, F.; Gullledge, D.; Wang, Q. *Tetrahedron Lett.* **2008**, 49, 5293-5296.

### Dianthryl-TTFV 1



Compound **2** (50.0 mg, 0.081 mmol), azido anthracene **3** (94.8 mg, 0.406 mmol) and  $i$ Pr<sub>2</sub>EtN (0.007 mL, 0.040 mmol) were dissolved in dry THF (5 mL). The solution was degassed by bubbling N<sub>2</sub> at rt for 5 min. Then CuI (1.54 mg, 0.0081 mmol) was added, and the reaction mixture was heated at 60°C for overnight. After the reaction mixture was completed as checked by TLC analysis, the solvent was removed under reduced pressure. The residue was diluted with CH<sub>2</sub>Cl<sub>2</sub>. The mixture was filtered through a MgSO<sub>4</sub> pad and the filtrate was sequentially washed with brine and water. The organic layer was dried over MgSO<sub>4</sub> and concentrated under vacuum to give crude **1**, which was further purified by silica flash column chromatography (EtOAc/hexanes, 3:7) to yield pure compound **1** (80.5 mg, 0.078 mmol, 91%) as a pale yellow solid. m.p. > 265 °C (decomp); IR (neat) : 2916, 2365, 1614, 1523, 1484, 1433, 1421, 1315, 1209, 1181, 1038, 966 cm<sup>-1</sup>; <sup>1</sup>H NMR (500 MHz, CDCl<sub>3</sub>): δ 8.59 (s, 2H), 8.32 (d, *J* = 8.9 Hz, 2H), 8.09 (d, *J* = 8.4 Hz, 2H), 7.61-7.49 (m, 14H), 7.25-7.20 (m, 2H), 6.55 (s, 2H), 2.34 (s, 2H), 2.29 (s, 2H); <sup>13</sup>C NMR (75 MHz, CDCl<sub>3</sub>): δ 147.4, 136.6, 136.3, 131.4, 130.8, 129.9, 129.4, 128.7, 127.9, 127.7, 126.8, 125.7, 125.4, 124.9, 124.0, 123.7, 122.9, 119.0, 46.4, 18.7; HRMS (MALDI-TOF, +eV) *m/z* calcd for C<sub>58</sub>H<sub>44</sub>N<sub>6</sub>S<sub>8</sub> 1080.1393, found 1080.1464 [M]<sup>+</sup>.

## 2. NMR Spectroscopic Data

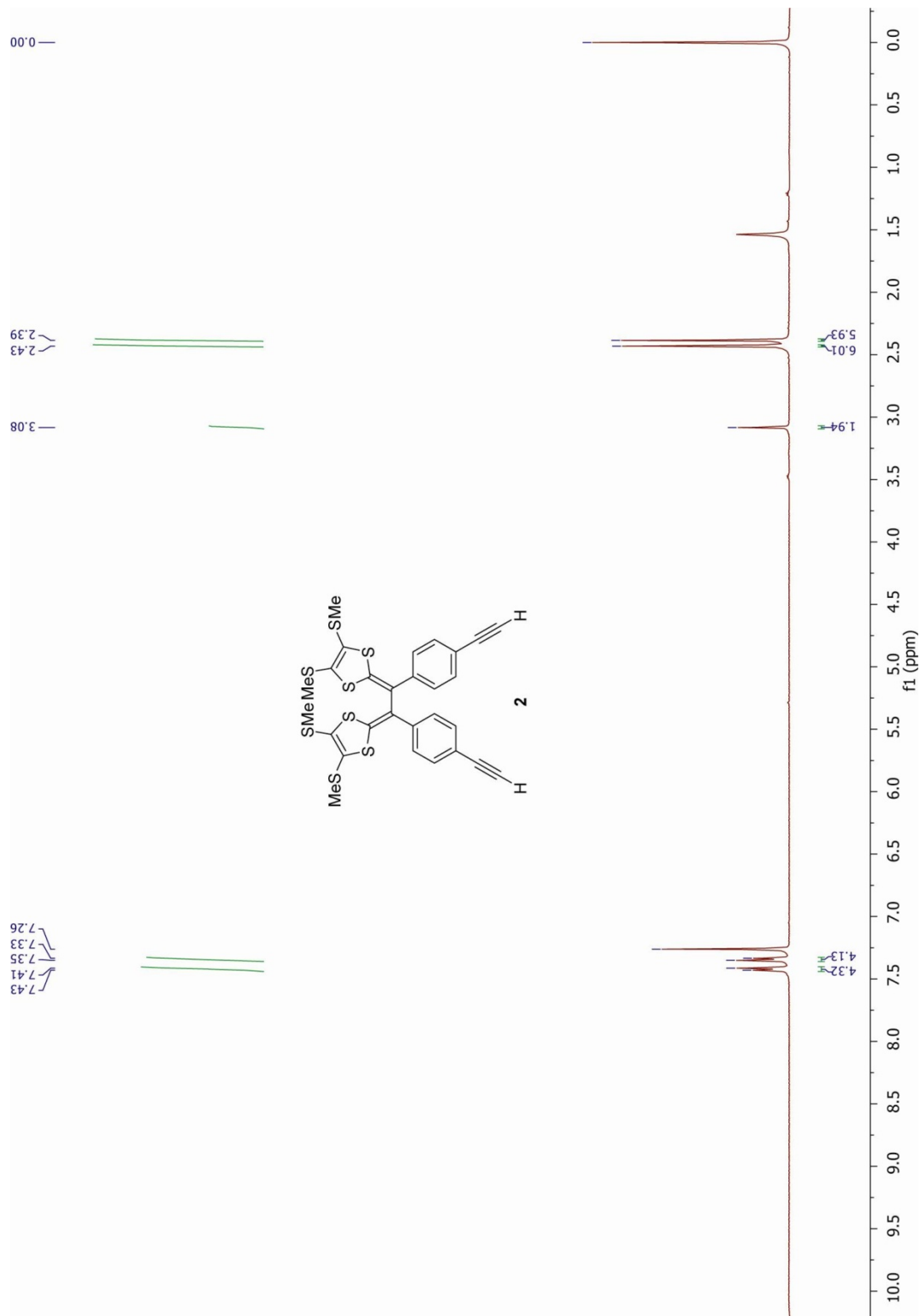


**Fig. S-1.**  $^1\text{H}$  NMR (500 MHz,  $\text{CDCl}_3$ ) spectrum of compound **2**.

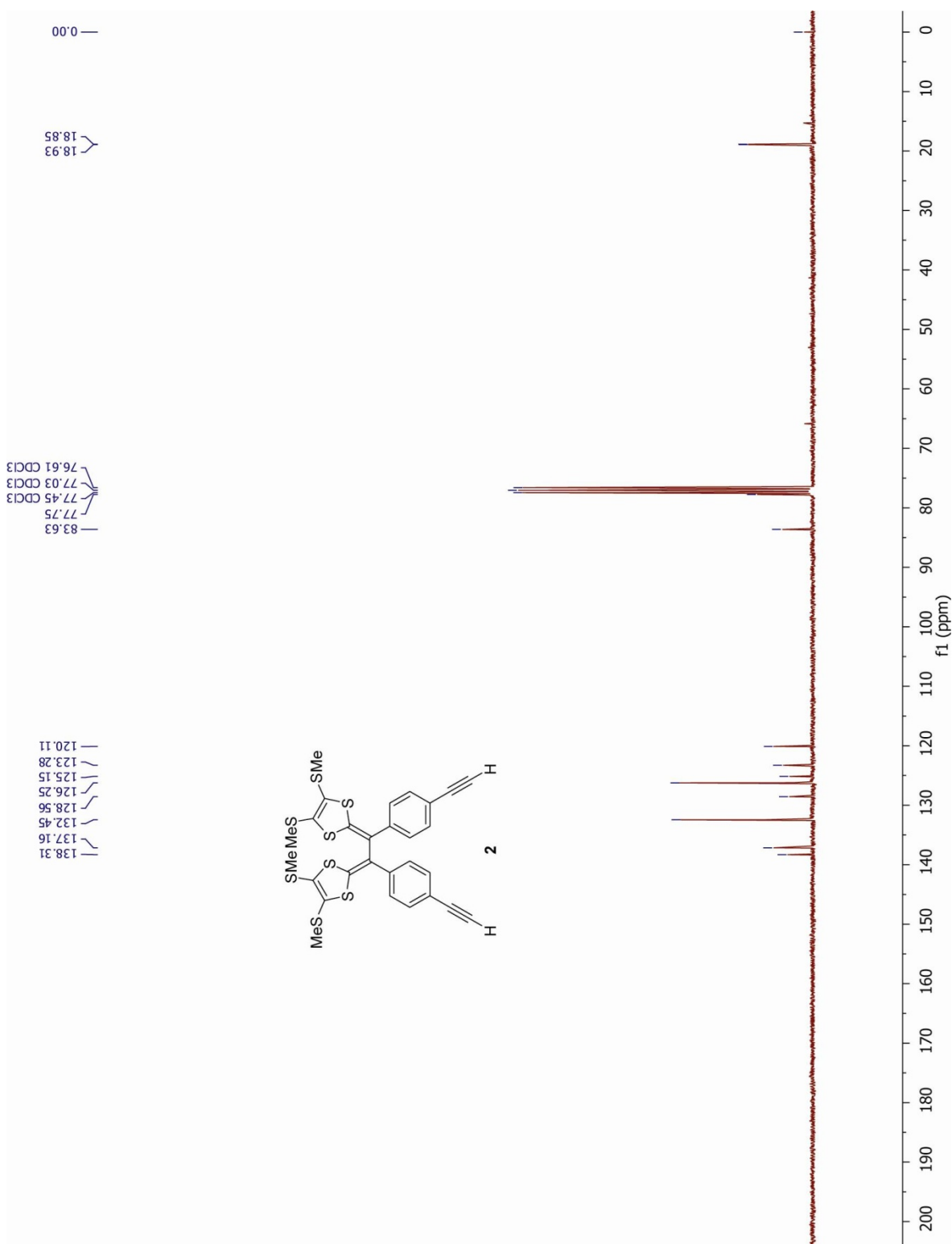


**Fig. S-2.**  $^{13}\text{C}$  NMR (125 MHz,  $\text{CDCl}_3$ ) spectrum of compound **2**.

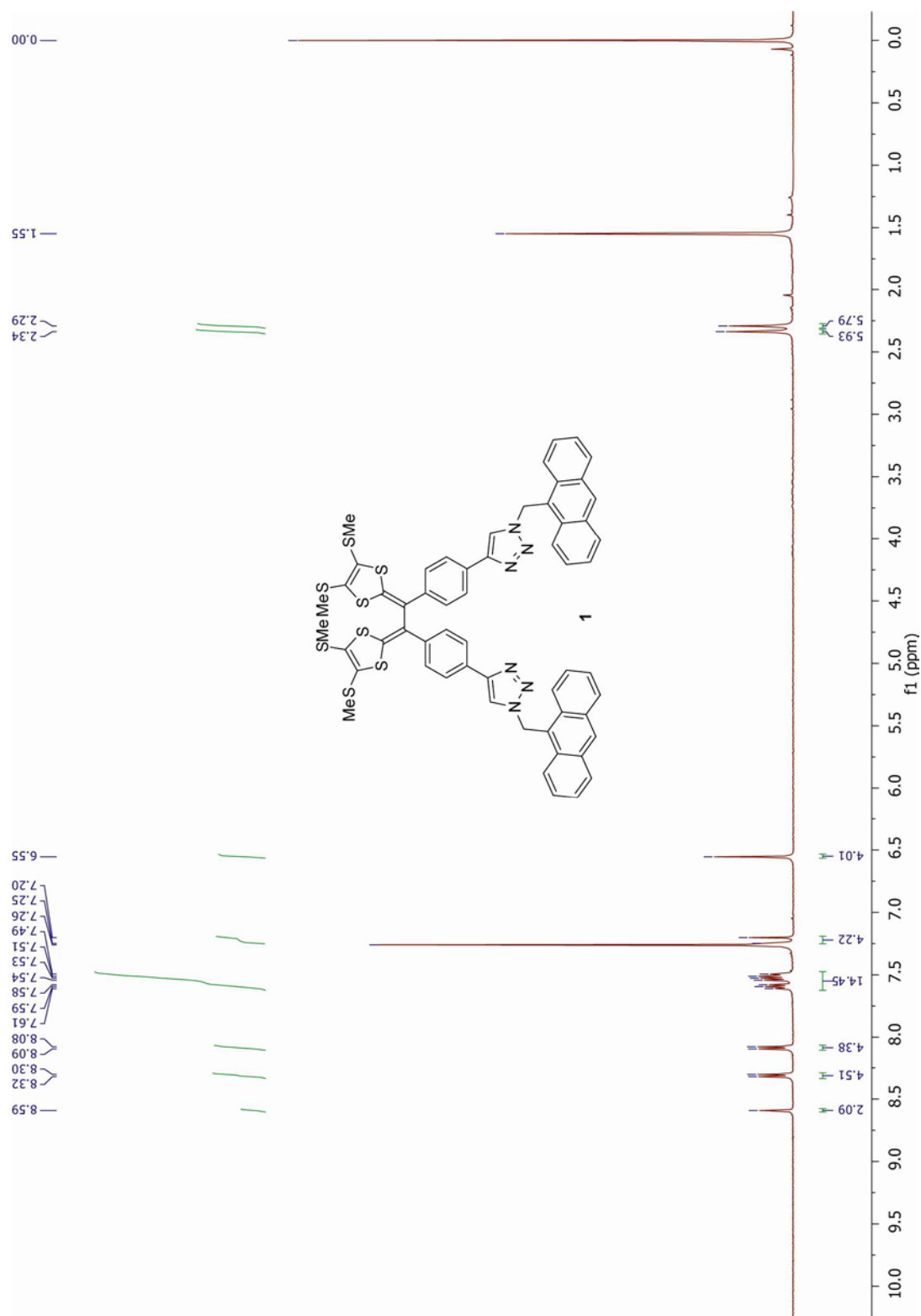


**Fig. S-3.** <sup>1</sup>H NMR (500 MHz, CDCl<sub>3</sub>) spectrum of compound **1**.

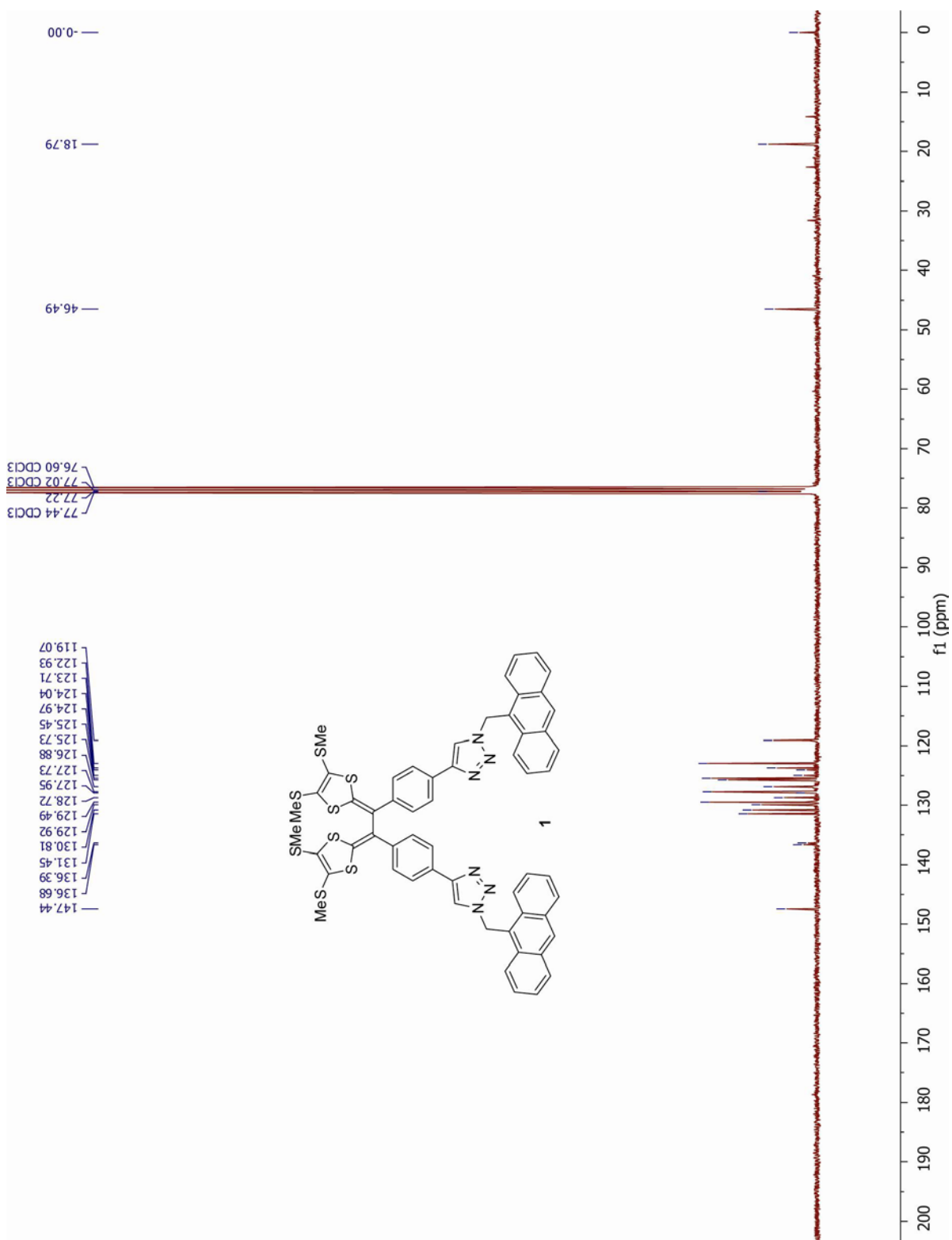
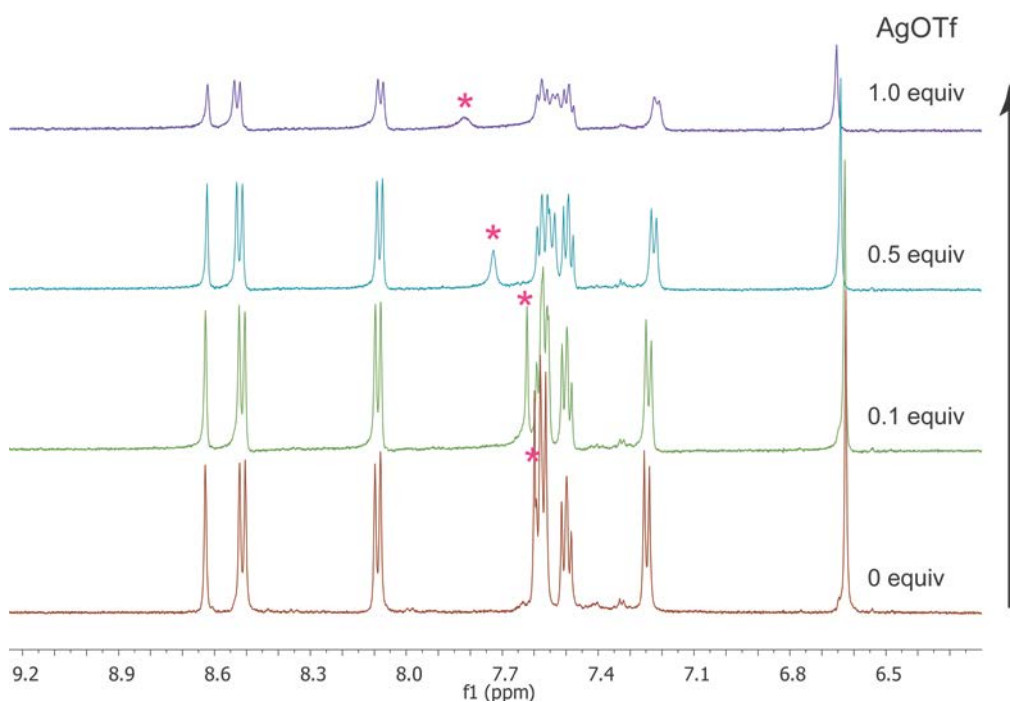
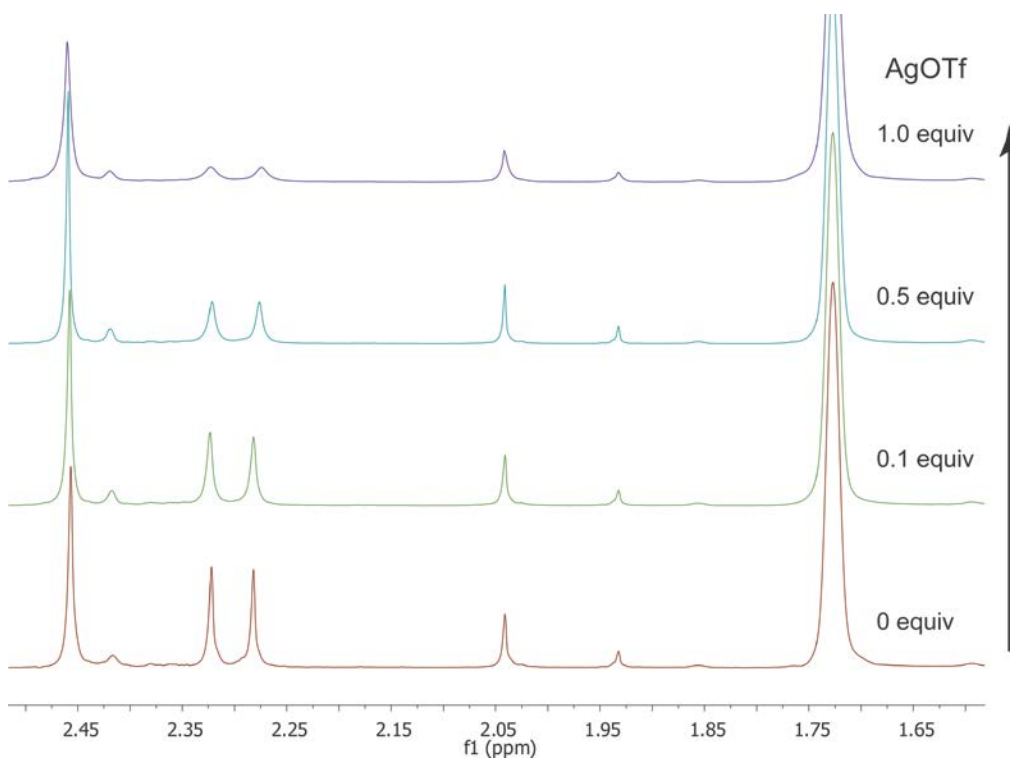


Fig. S-4.  $^{13}\text{C}$  NMR (75 MHz,  $\text{CDCl}_3$ ) spectrum of compound 1.



**Fig. S-5.** Partial <sup>1</sup>H NMR spectra of compound **1** (7.4 mM) in titration with AgOTf in THF-*d*<sub>8</sub> showing the aromatic region. Signals labeled by \* refers to the triazolyl proton.



**Fig. S-6.** Partial <sup>1</sup>H NMR spectra of compound **1** (7.4 mM) in titration with AgOTf in THF-*d*<sub>8</sub> showing the aliphatic region.

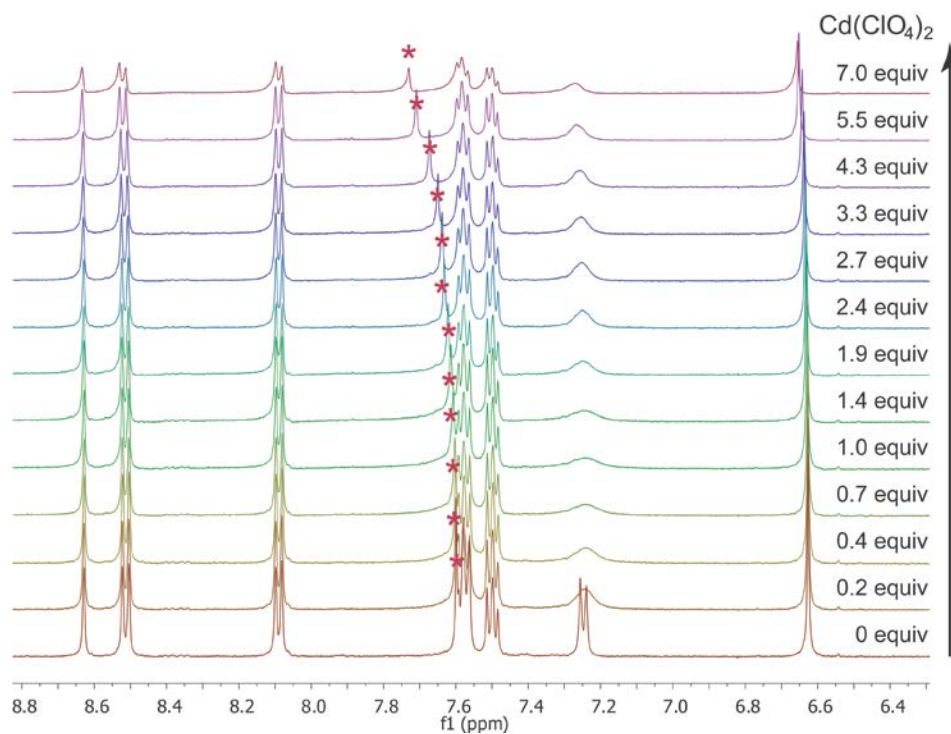


**Fig. S-7.** Partial <sup>1</sup>H NMR spectra of compound **1** (7.4 mM) in titration with Cd(ClO<sub>4</sub>)<sub>2</sub> in THF-*d*<sub>8</sub> showing the aromatic region. Signals labeled by \* refers to the triazolyl proton.

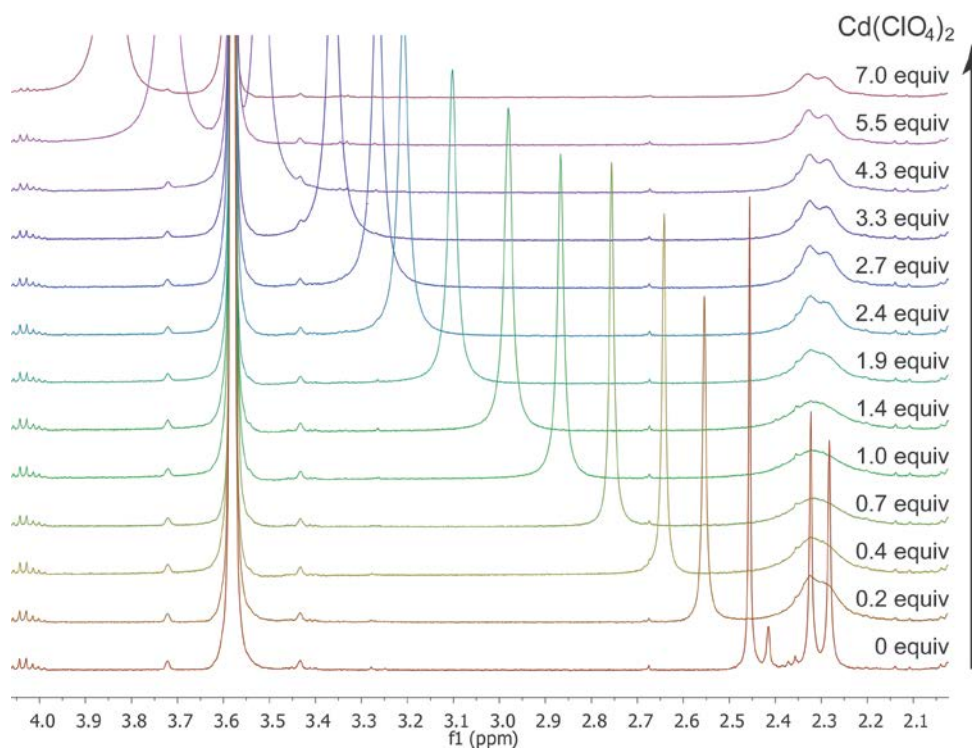


**Fig. S-8.** Partial <sup>1</sup>H NMR spectra of compound **1** (7.4 mM) in titration with Cd(ClO<sub>4</sub>)<sub>2</sub> in THF-*d*<sub>8</sub> showing the aliphatic region.

From the  $^1\text{H}$  NMR titration results of  $\text{Cu}^{2+}$  and  $\text{Ag}^+$ , it is clearly seen that the triazolyl protons (labeled by \* in Figures S-5 and S-7) show the most significant downfield shift, while other signals barely change. The two singlets around 2.3 ppm (Figures S-6 and S-9), assigned to the  $\text{SCH}_3$ , do not show any shift but become broadened as the titration progresses. These observations indicate that the major metal ion binding sites are the triazole units, however, the possibility of  $\text{SCH}_3$  might weakly interacting with metal ions cannot be ruled out. Based on the NMR titration results and the stoichiometry measured from UV-Vis analysis (vide infra), a binding model is tentatively proposed as follows.

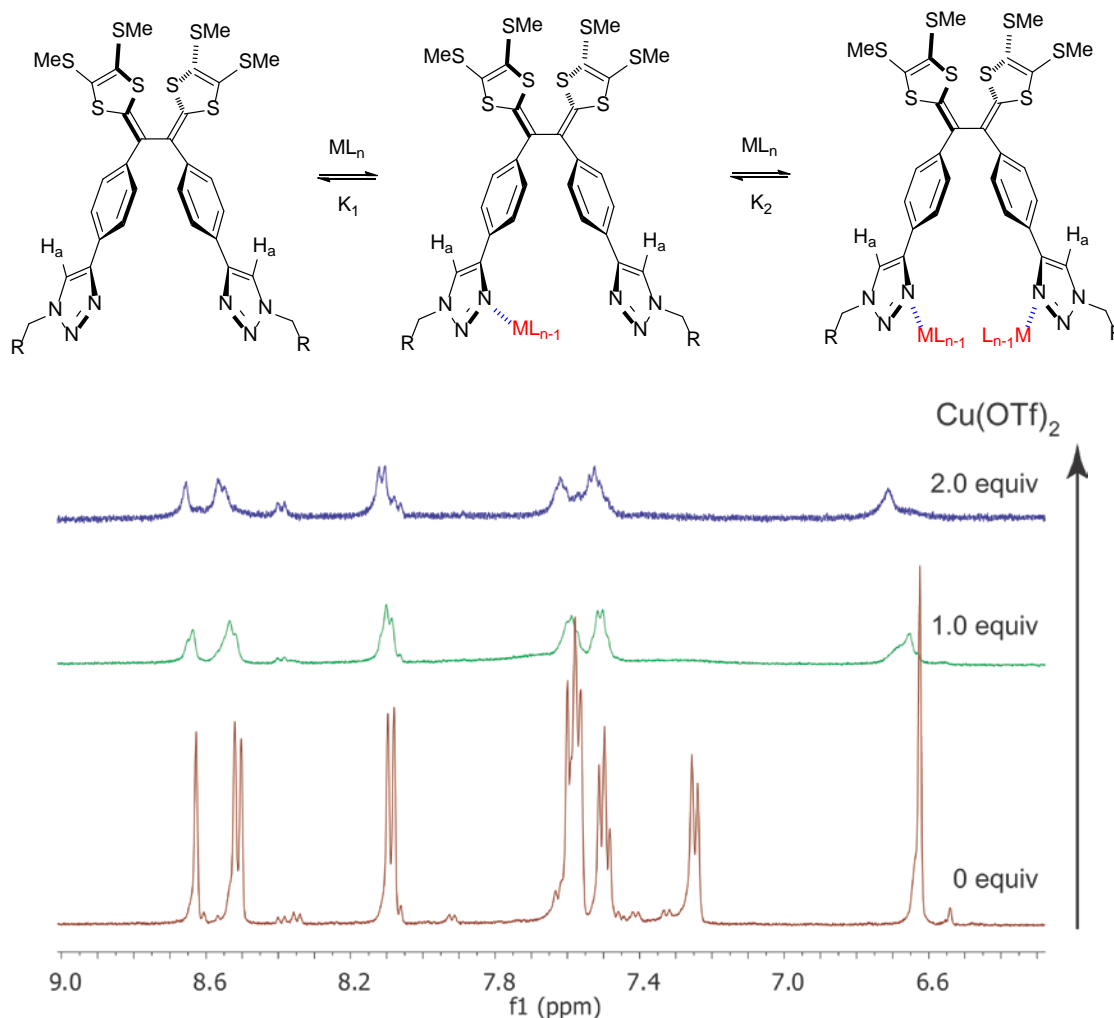


**Fig. S-9.** Partial  $^1\text{H}$  NMR titration of compound 1 (7.4 mM) with  $\text{Cu}(\text{OTf})_2$  in  $\text{THF-}d_8$  showing the aromatic region.

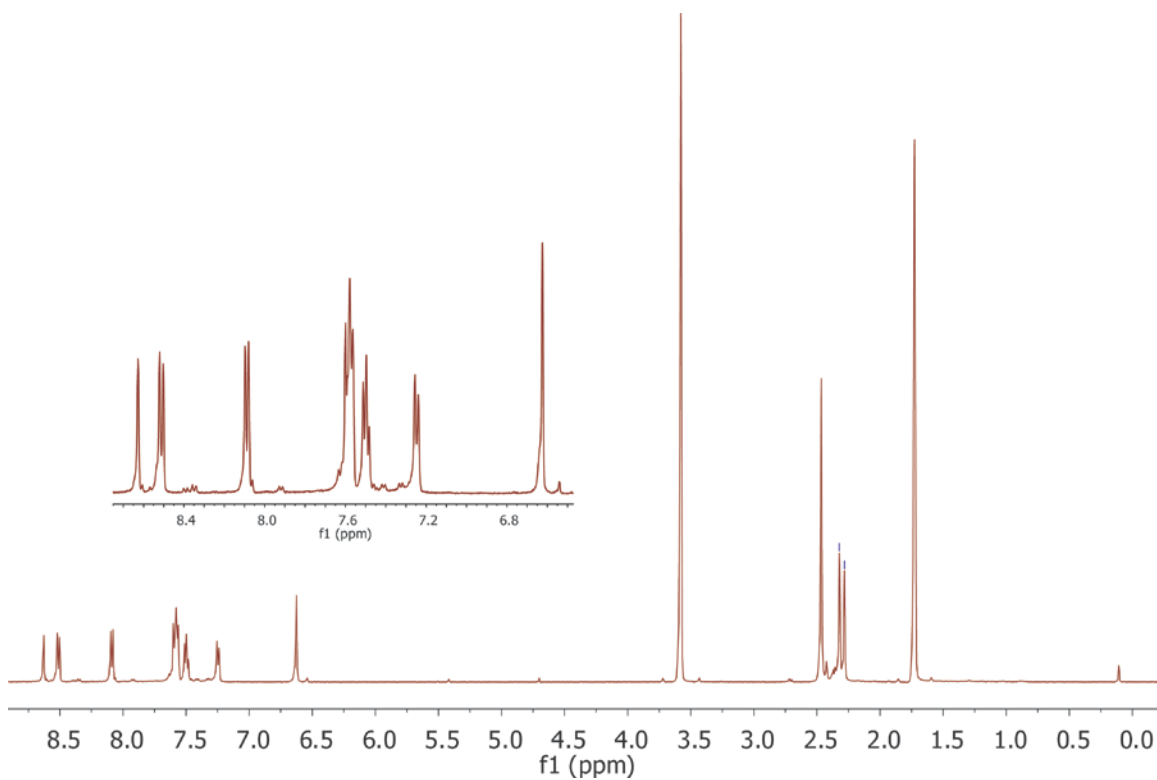


**Fig. S-10.** <sup>1</sup>H NMR (500 MHz, CD<sub>3</sub>CN) spectrum of compound **1** complexed with 2 mol equiv of Cu(OTf)<sub>2</sub>.

### 3. UV-Vis and Fluorescence Spectral Data

#### 3.1 Steady-state measurements

UV-Visible spectra were recorded on an Agilent 8543 Diode Array Spectrophotometer interfaced to an HP computer. Data manipulations were conducted using software supplied by the manufacturer. Spectroscopic experiments were conducted using 1cm sealed quartz fluorescence cuvettes supplied by Aldrich.

Emission spectra were measured on a Photon Technology International (PTI) Quantamaster 6000 spectrofluorometer equipped with a continuous xenon arc lamp as the excitation source. The emitting light was collected at 90° to the excitation beam and detected by a Hamamatsu R-928 photomultiplier tube (PMT) in photon counting mode. The PMT was housed in a water-cooled PMT housing supplied by Products for Research Inc. All emission spectra were corrected for instrumental light loss using correction factors supplied by PTI.

**Reagents.** All the metal ion salts were received from Sigma Aldrich in >99 % purity. High-purity spectral grade THF was supplied by sigma Aldrich and used as received.

**Titration procedure.** In a typical experiment fixed molar solutions of **1** in THF were prepared by gravimetric methods for each individual experiment. The concentration of **1** was set between 5.0 to 6.0 μM for titrations. Stock solutions of individual metal salts were also prepared by gravimetric methods in THF (unless otherwise noted). The concentration of each stock solution was different and set according to its response towards the sensor observed in the preliminary experiments. AgOTf was dissolved in CHCl<sub>3</sub> and Zn(OTf)<sub>2</sub> was dissolved in CH<sub>3</sub>CN for achieving best solubility.

Aliquots from previously prepared stock solution of **1** was added to cuvette containing 2.50 mL of THF to achieve the desired concentration (5 to 6 μM). After acquiring the absorption and emission spectra of **1**, solutions of metal salts were added using a micro-syringe (supplied by Hamilton). Addition of aliquots of metal salts in THF resulted in spectral changes in absorption and emission spectra assigned to sequential binding reactions of **1** with cations. The resulting data was saved in appropriate format and plotted using Origin 8.0 (Origin Lab corporation).

Emission quantum yields were measured in N<sub>2</sub> saturated THF solutions at 295 ± 3 K. The absorbance of the samples < 0.2 at the excitation wavelength ( $\lambda_{\text{exc}} = 350 \text{ nm}$ ) to

prevent distortion of the emission spectral data by inner-filter effects. The radiative quantum yields for all compounds ( $\lambda_{em}$ ) were determined using quinine bisulfate in 0.1 M aqueous sulfuric acid solution as the actinometer ( $\lambda_{std} = 0.52$  at  $\lambda_{exc} = 350$  nm) and calculated according to equation S-1,

$$\phi_{em} = \phi_{std} \left( \frac{A_{std}}{A_{un}} \right) \left( \frac{I_{un}}{I_{std}} \right) \left( \frac{n_{un}}{n_{std}} \right)^2 \quad [S-1]$$

where  $A$  is the solution absorbance,  $I$  the emission intensity,  $n$  the refraction index of the solvent, and the subscripts  $un$  and  $std$  refers to the unknown and standard respectively.

### 3.2 Spectroscopic titration data

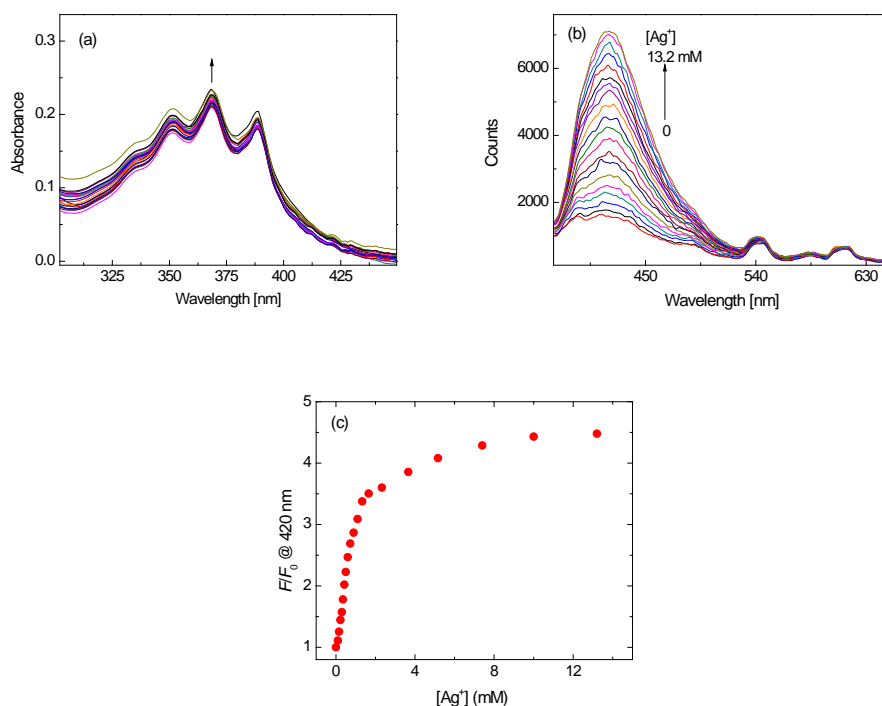


**Fig. S-11.** (a) UV-Vis absorption (b) fluorescence spectra of **1** ( $5.92 \mu\text{M}$ ,  $\lambda_{ex} = 350$  nm) obtained as a function of increasing concentration of AgOTf in THF at  $298 \pm 3$  K. The arrows indicate the trend for increasing AgOTf. (c) The plot of  $(F/F_0)$  vs  $[AgOTf]$  determined at 420 nm ( $\lambda_{ex} = 350$  nm).  $F/F_0$  denotes the ratio between observed fluorescence intensity and initial fluorescence intensity.

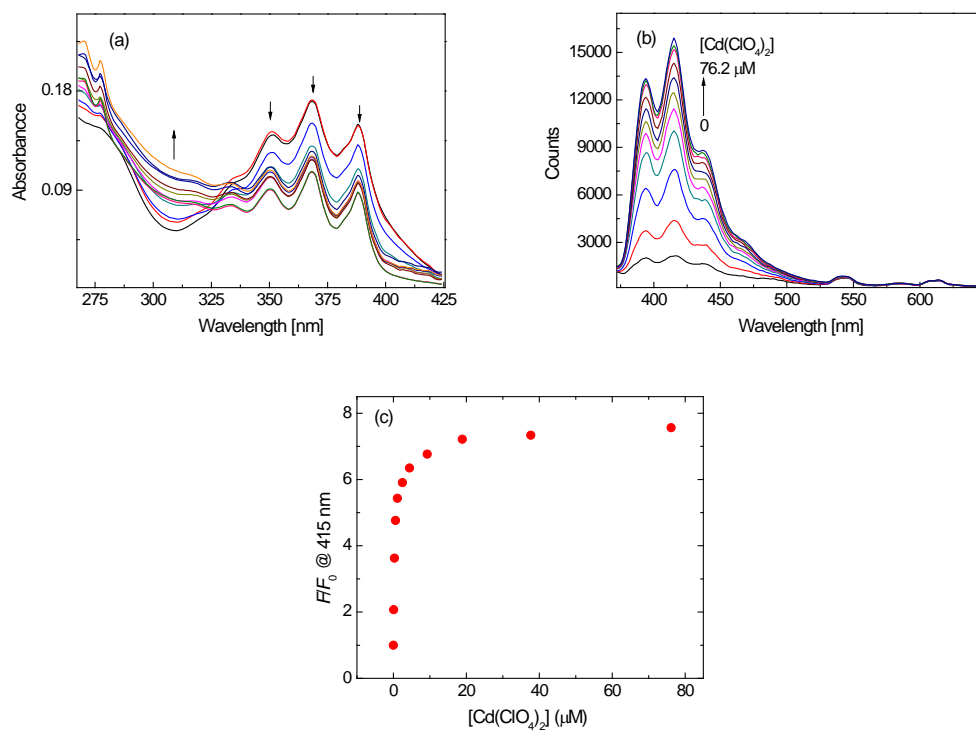


**Fig. S-12.** (a) UV-Vis absorption, (b) fluorescence spectra of **1** (5.52  $\mu\text{M}$ ,  $\lambda_{ex} = 350$  nm) obtained as a function of increasing concentration of  $\text{Cd}(\text{ClO}_4)_2$  in THF at  $298 \pm 3$  K. The arrows indicate the trend for increasing  $\text{Cd}(\text{ClO}_4)_2$ . (c) The plot of  $(F/F_0)$  vs  $[\text{Cd}(\text{ClO}_4)_2]$  determined at 415 nm ( $\lambda_{ex} = 350$  nm).  $F/F_0$  denotes the ratio between observed fluorescence intensity and initial fluorescence intensity.

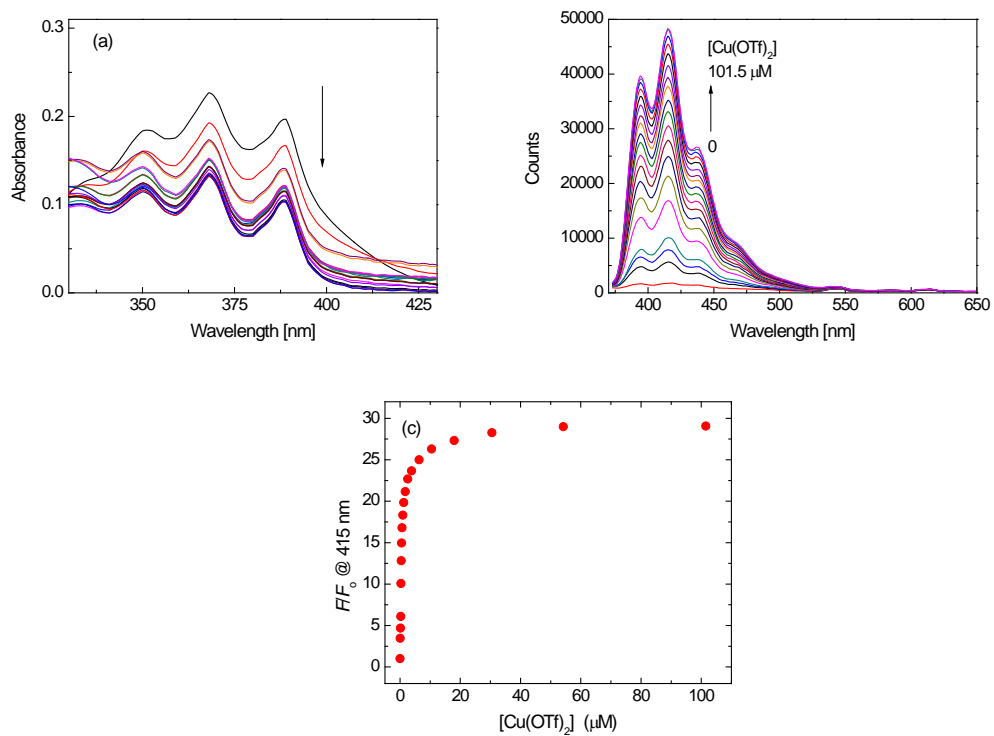


**Fig. S-13.** (a) UV-Vis absorption, (b) fluorescence spectra of **1** ( $5.55 \mu\text{M}$ ,  $\lambda_{ex} = 350 \text{ nm}$ ) obtained as a function of increasing concentration of  $\text{Cu}(\text{OTf})_2$  in THF at  $298 \pm 3 \text{ K}$ . The arrows indicate the trend for increasing  $\text{Cu}(\text{OTf})_2$ . (c) The plot of  $(F/F_0)$  vs  $[\text{Cu}(\text{OTf})_2]$  determined at  $415 \text{ nm}$  ( $\lambda_{ex} = 350 \text{ nm}$ ).  $F/F_0$  denotes the ratio between observed fluorescence intensity and initial fluorescence intensity.

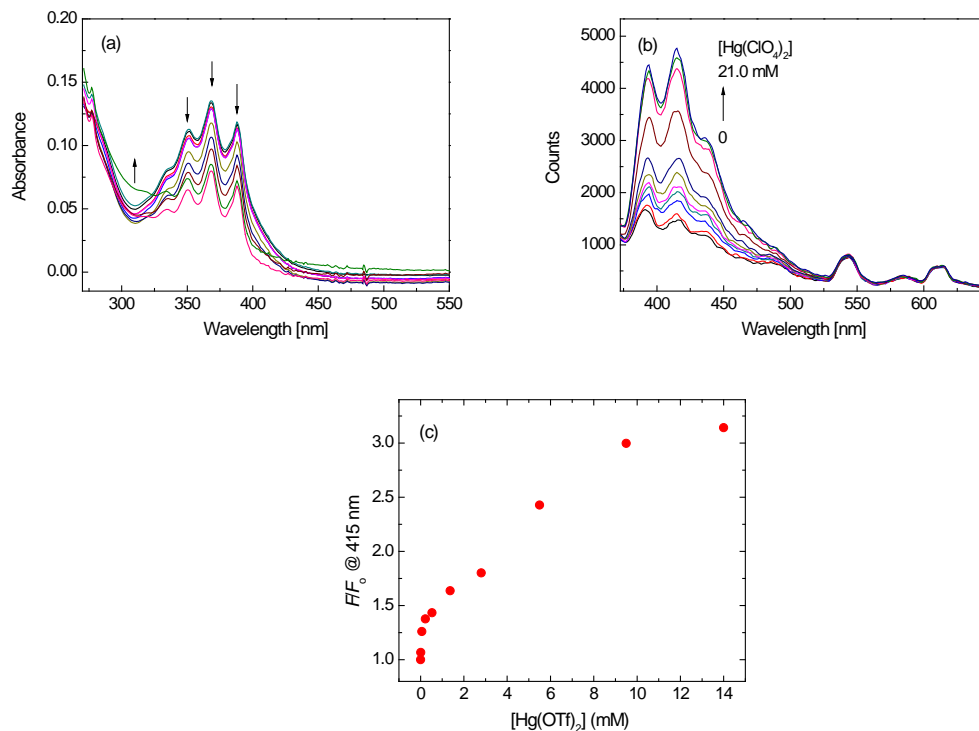


**Fig. S-14.** (a) UV-Vis absorption, (b) fluorescence spectra of **1** ( $5.09 \mu\text{M}$ ,  $\lambda_{ex} = 350 \text{ nm}$ ) obtained as a function of increasing concentration of  $\text{Hg}(\text{ClO}_4)_2$  in THF at  $298 \pm 3 \text{ K}$ . The arrows indicate the trend for increasing  $\text{Hg}(\text{ClO}_4)_2$ . (c) The plot of  $(F/F_0)$  vs  $[\text{Hg}(\text{ClO}_4)_2]$  determined at  $415 \text{ nm}$  ( $\lambda_{ex} = 350 \text{ nm}$ ).  $F/F_0$  denotes the ratio between observed fluorescence intensity and initial fluorescence intensity.

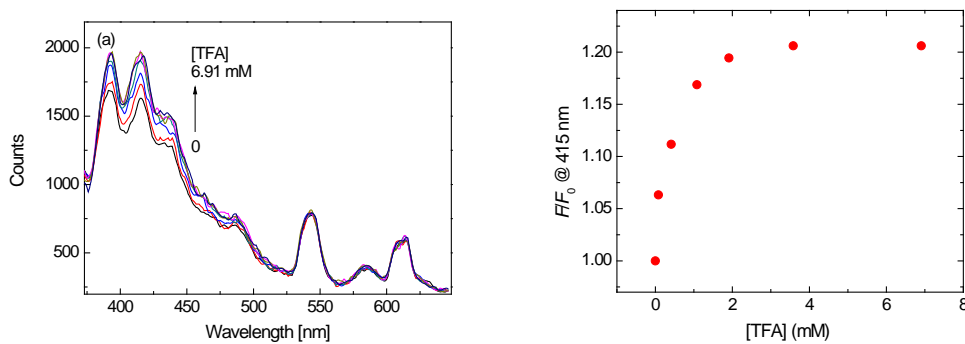


**Fig. S-15.** (a) Fluorescence spectra of **1** ( $5.00 \mu\text{M}$ ,  $\lambda_{ex} = 350 \text{ nm}$ ) obtained as a function of increasing concentration of TFA in THF at  $298 \pm 3 \text{ K}$ . The arrows indicate the trend for increasing TFA. (b) The plot of  $(F/F_0)$  vs [TFA] determined at  $415 \text{ nm}$  ( $\lambda_{ex} = 350 \text{ nm}$ ).  $F/F_0$  denotes the ratio between observed fluorescence intensity and initial fluorescence intensity.

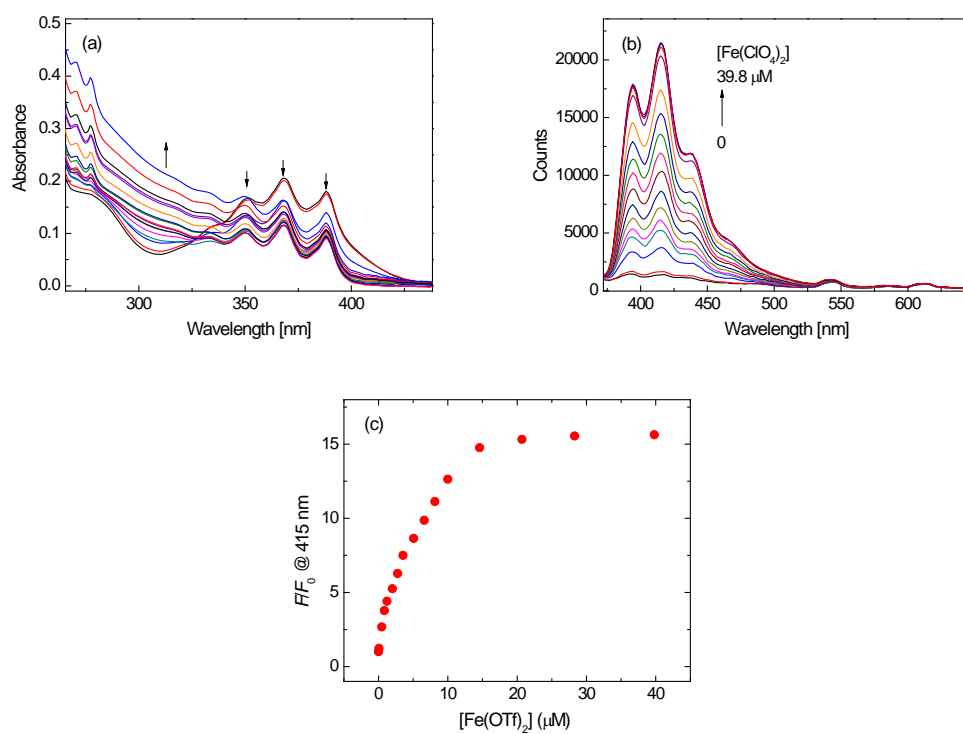


**Fig. S-16.** (a) UV-Vis absorption, (b) fluorescence spectra of **1** (5.45  $\mu\text{M}$ ,  $\lambda_{ex} = 350 \text{ nm}$ ) obtained as a function of increasing concentration of  $\text{Fe}(\text{ClO}_4)_2$  in THF at  $298 \pm 3 \text{ K}$ . The arrows indicate the trend for increasing  $\text{Fe}(\text{ClO}_4)_2$ . (c) The plot of  $(F/F_0)$  vs  $[\text{Fe}(\text{ClO}_4)_2]$  determined at 415 nm ( $\lambda_{ex} = 350 \text{ nm}$ ).  $F/F_0$  denotes the ratio between observed fluorescence intensity and initial fluorescence intensity.

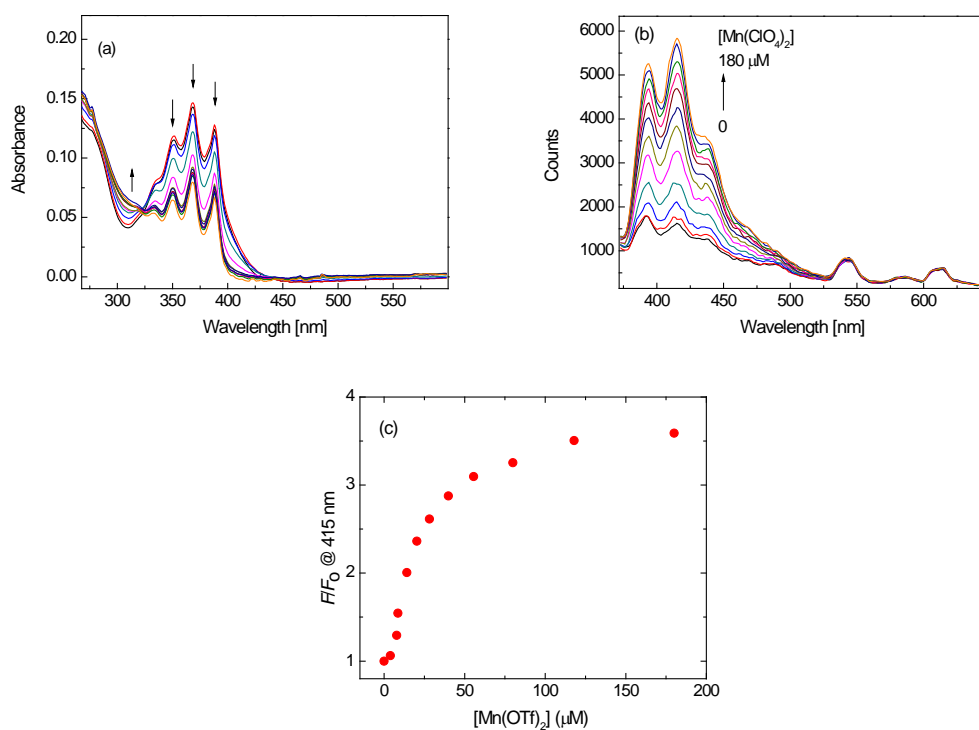


**Fig. S-17.** (a) UV-Vis absorption, (b) fluorescence spectra of **1** ( $5.51 \mu\text{M}$ ,  $\lambda_{ex} = 350 \text{ nm}$ ) obtained as a function of increasing concentration of  $\text{Mn}(\text{ClO}_4)_2$  in THF at  $298 \pm 3 \text{ K}$ . The arrows indicate the trend for increasing  $\text{Mn}(\text{ClO}_4)_2$ . (c) The plot of  $(F/F_0)$  vs  $[\text{Mn}(\text{ClO}_4)_2]$  determined at  $415 \text{ nm}$  ( $\lambda_{ex} = 350 \text{ nm}$ ).  $F/F_0$  denotes the ratio between observed fluorescence intensity and initial fluorescence intensity.

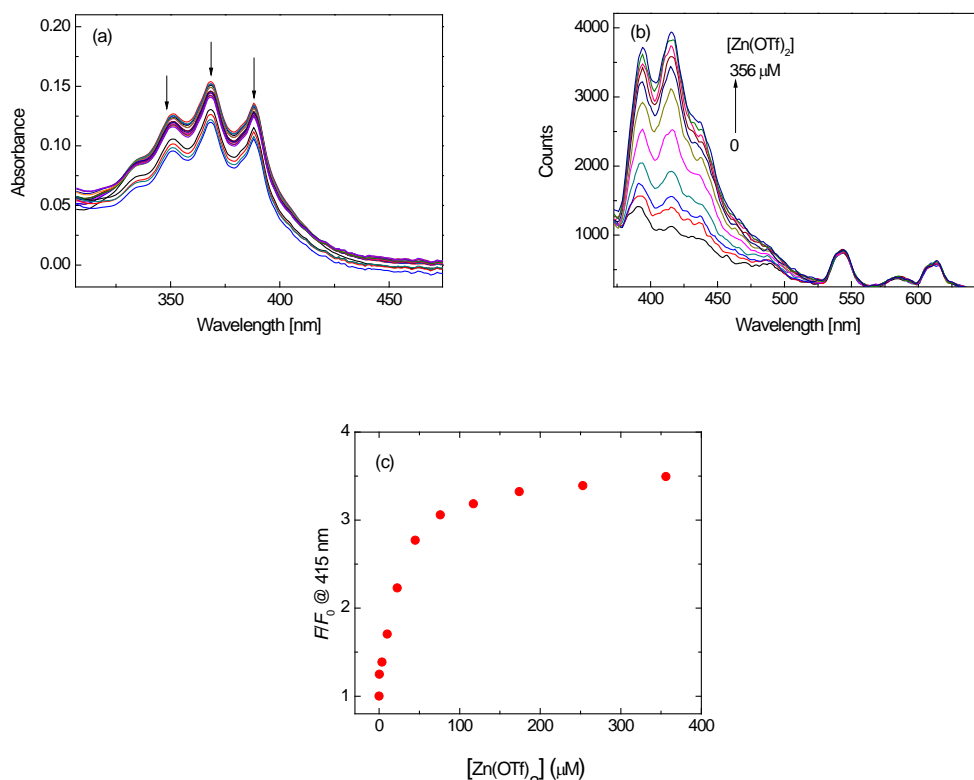


**Fig. S-18.** (a) UV-Vis absorption, (b) fluorescence spectra of **1** (5.57  $\mu\text{M}$ ,  $\lambda_{ex} = 350$  nm) obtained as a function of increasing concentration of  $\text{Zn}(\text{OTf})_2$  in THF at  $298 \pm 3$  K. The arrows indicate the trend for increasing  $\text{Zn}(\text{OTf})_2$ . (c) The plot of  $(F/F_0)$  vs  $[\text{Zn}(\text{OTf})_2]$  determined at 415 nm ( $\lambda_{ex} = 350$  nm).  $F/F_0$  denotes the ratio between observed fluorescence intensity and initial fluorescence intensity.

### 3.3 Determination of binding constants by SPECFIT

Binding constants were extracted by using the SPECFIT/32 program. Emission data obtained from titration experiments were subjected to the global spectral fitting analysis implemented in SPECFIT to extract binding constants and related concentration profiles.

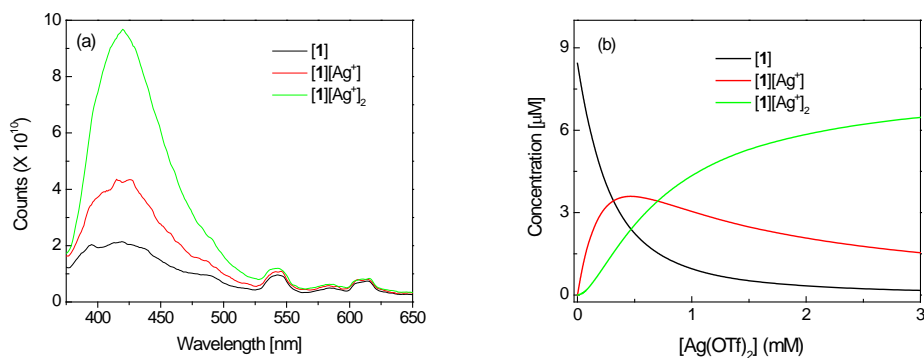


**Fig. S-19.** (a) Deconvoluted emission spectra of colorful species involved in the titration of **1** with AgOTf. (b) Correlation between the concentrations of colorful species and [Ag<sup>+</sup>].  $\log \beta_{11} = 3.57 \pm 0.1 \text{ M}^{-1}$ ;  $\log \beta_{12} = 6.67 \pm 0.1 \text{ M}^{-2}$ .

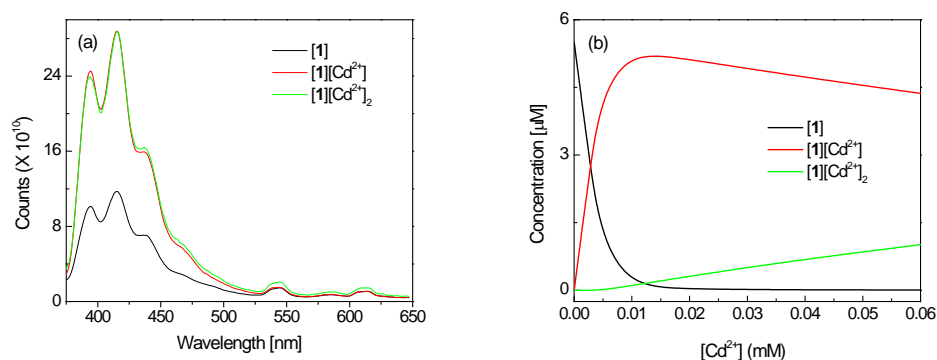


**Fig. S-20.** (a) Deconvoluted emission spectra of colorful species involved in the titration of **1** with Cd(ClO<sub>4</sub>)<sub>2</sub>. (b) Correlation between the concentrations of colorful species and [Cd<sup>2+</sup>].  $\log \beta_{11} = 5.22 \pm 0.6 \text{ M}^{-1}$ ;  $\log \beta_{12} = 9.75 \pm 0.6 \text{ M}^{-2}$ .

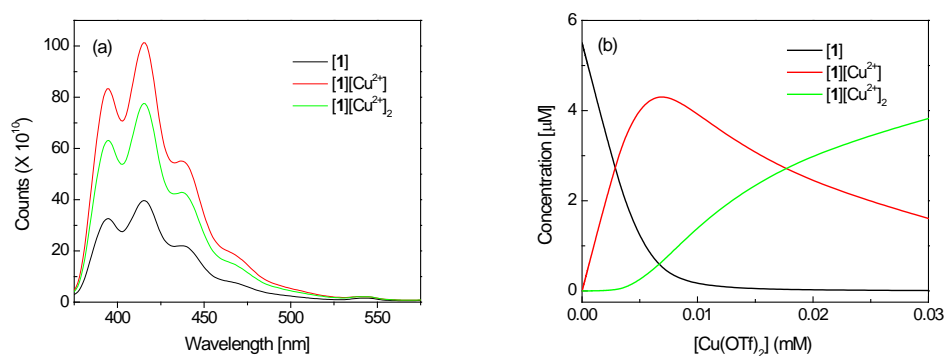


**Fig. S-21.** (a) Deconvoluted emission spectra of colorful species involved in the titration of **1** with Cu(OTf)<sub>2</sub>. (b) Correlation between the concentrations of colorful species and [Cu<sup>2+</sup>].  $\log \beta_{11} = 7.12 \pm 0.7 \text{ M}^{-1}$ ;  $\log \beta_{12} = 12.1 \pm 0.8 \text{ M}^{-2}$ .

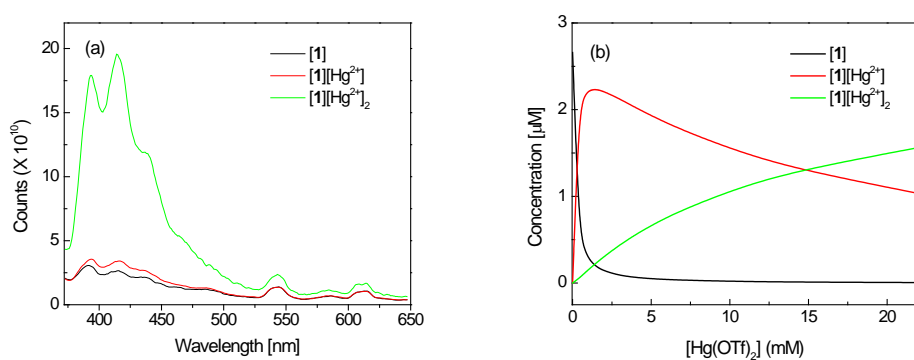


**Fig. S-22.** (a) Deconvoluted emission spectra of colorful species involved in the titration of **1** with Hg(ClO<sub>4</sub>)<sub>2</sub>. (b) Correlation between the concentrations of colorful species and [Hg<sup>2+</sup>].  $\log \beta_{11} = 2.72 \pm 0.2 \text{ M}^{-1}$ ;  $\log \beta_{12} = 4.47 \pm 0.2 \text{ M}^{-2}$ .

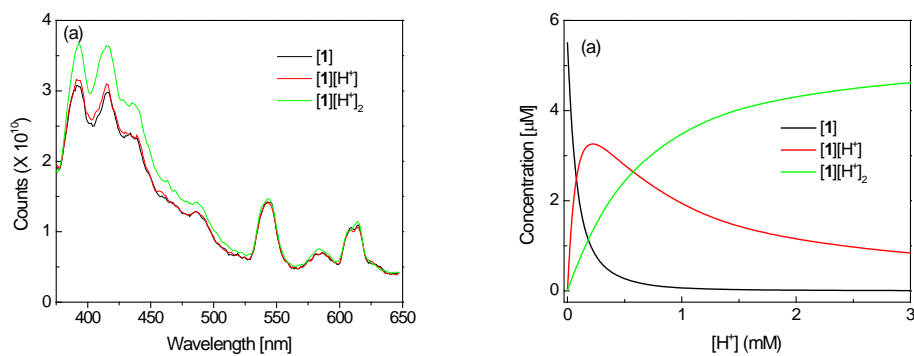


**Fig. S-23.** (a) Deconvoluted emission spectra of colorful species involved in the titration of **1** with TFA. (b) Correlation between the concentrations of colorful species and [H<sup>+</sup>].  $\log \beta_{11} = 1.63 \pm 0.5 \text{ M}^{-1}$ ;  $\log \beta_{12} = 2.95 \pm 0.6 \text{ M}^{-2}$ .

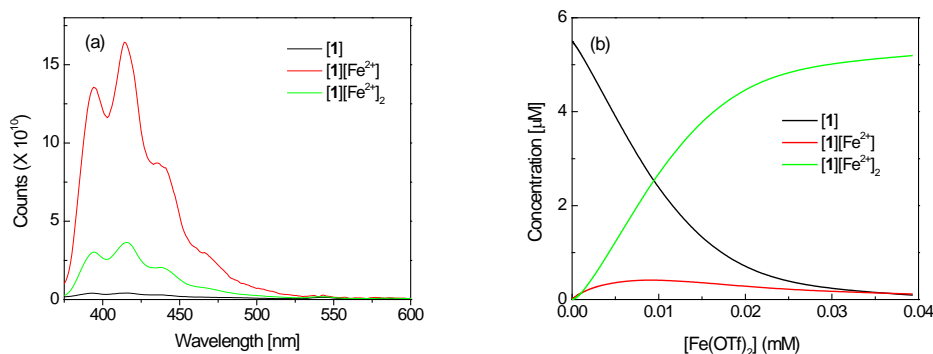


**Fig. S-24.** (a) Deconvoluted emission spectra of colorful species involved in the titration of **1** with Fe(ClO<sub>4</sub>)<sub>2</sub>. (b) Correlation between the concentrations of colorful species and [Fe<sup>2+</sup>].  $\log \beta_{11} = 4.62 \pm 0.4 \text{ M}^{-1}$ ;  $\log \beta_{12} = 10.8 \pm 0.2 \text{ M}^{-2}$ .

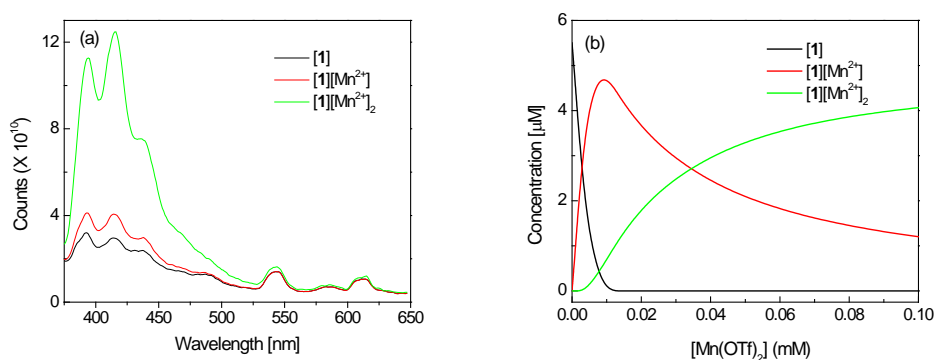


**Fig. S-25.** (a) Deconvoluted emission spectra of colorful species involved in the titration of **1** with Mn(ClO<sub>4</sub>)<sub>2</sub>. (b) Correlation between the concentrations of colorful species and [Mn<sup>2+</sup>].  $\log \beta_{11} = 4.58 \pm 0.1 \text{ M}^{-1}$ ;  $\log \beta_{12} = 7.56 \pm 0.1 \text{ M}^{-2}$ .

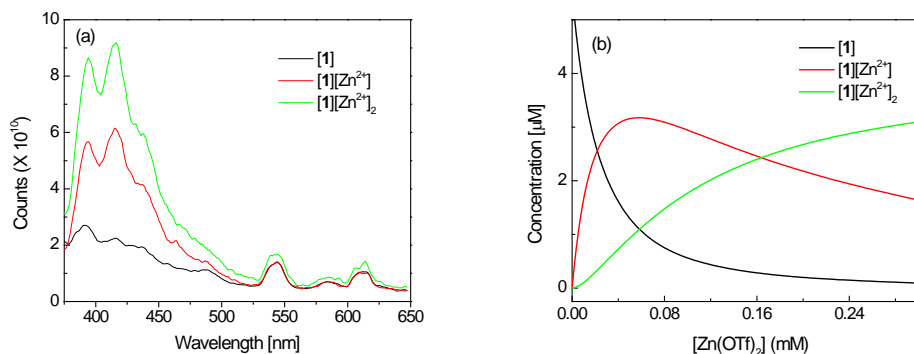


**Fig. S-26.** (a) Deconvoluted emission spectra of colorful species involved in the titration of **1** with Zn(OTf)<sub>2</sub>. (b) Correlation between the concentrations of colorful species and [Zn<sup>2+</sup>].  $\log \beta_{11} = 4.78 \pm 0.2 \text{ M}^{-1}$ ;  $\log \beta_{12} = 8.59 \pm 0.3 \text{ M}^{-2}$ .

### 3.4 UV-Vis titration of TTFV precursor **4** with TFA and transition metal salts

To understand the electronic absorption features arising from the complexation between the TTFV moiety and  $H^+$  or various transition metal ions, UV-Vis titration experiments were carried out by adding  $H^+$ ,  $Cu^{2+}$ ,  $Cd^{2+}$ , and  $Fe^{2+}$  respectively to the solution of TTFV **4** in THF.

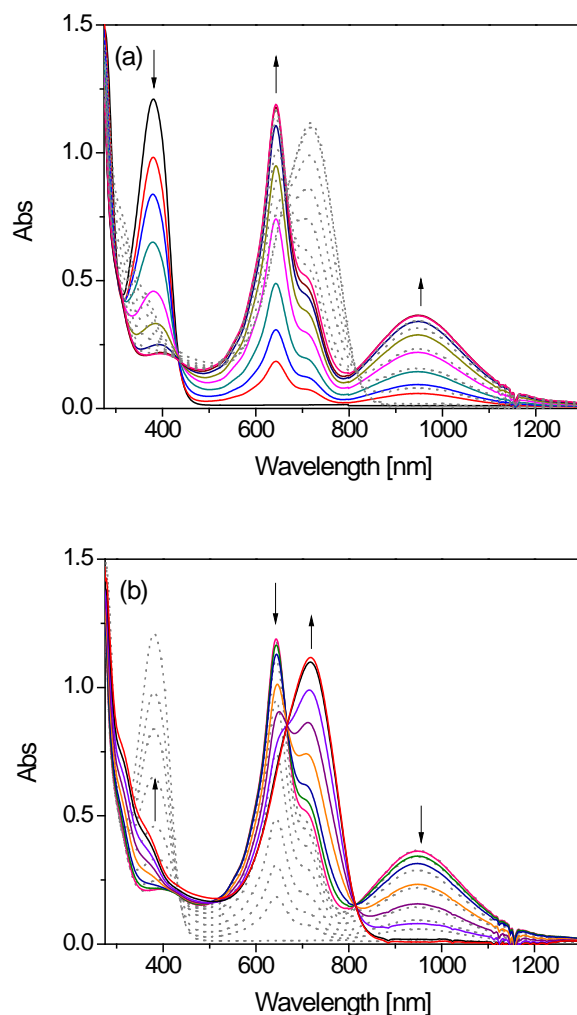


**Fig. S-27.** UV-Vis titration of TTFV **4** (40  $\mu$ M) with TFA in  $CHCl_3$ . (a) Addition of TFA from 0 to 16,000 molar equivalents. (b) Addition of TFA from 16,000 to molar 70,000 equivalents.

Note that in Figure S-27a, the emerging bands at 643 nm and 950 nm are assigned to monoprotonated species,  $[TTFV+H]^+$ . As titration progresses these two bands decrease and another absorption band grows at 719 nm, which is assigned to diprotonated species,  $[TTFV+2H]^{2+}$ . UV-Vis pectroelectrochemical analysis on TTFV **4** indicates that the absorption band in the range of ca. 600 to 800 nm is due to  $[TTFV]^{2+}$ . For details, see

reference: Chen, G.; Mahmud, I.; Dawe, L. N.; Daniels, L. M.; Zhao, Y. *J. Org. Chem.* **2011**, *76*, 2701-2715.

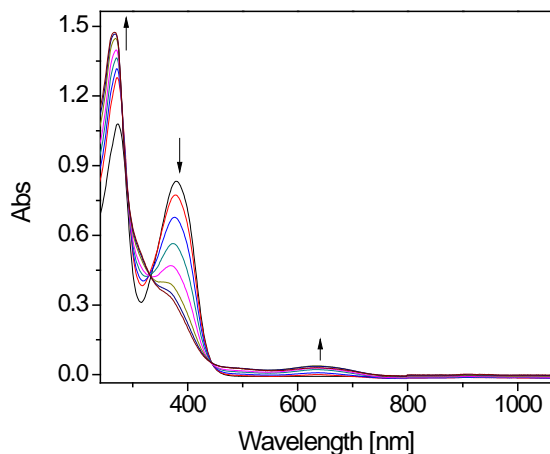


**Fig. S-28.** UV-Vis titration of TTFV **4** (26 μM) with Cu(OTf)<sub>2</sub> in THF. Addition of Cu(OTf)<sub>2</sub> from 0 to 18.2 molar equivalents.

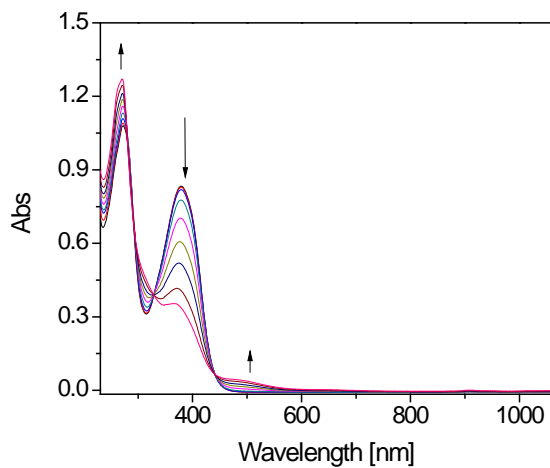


**Fig. S-29.** UV-Vis titration of TTFV **4** (26 μM) with Cd(ClO<sub>4</sub>)<sub>2</sub> in THF. Addition of Cd(ClO<sub>4</sub>)<sub>2</sub> from 0 to 56.0 molar equivalents.

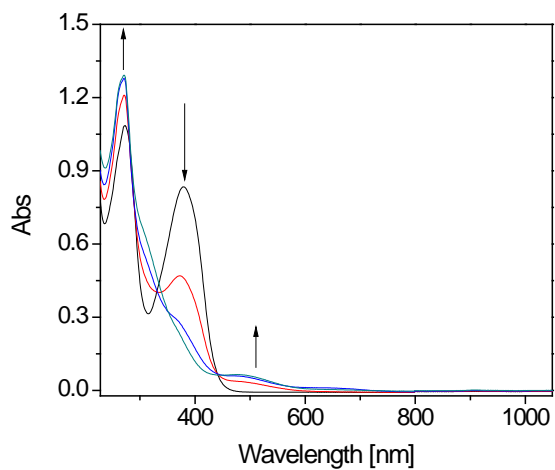


**Fig. S-30.** UV-Vis titration of TTFV **4** (26 μM) with Fe(ClO<sub>4</sub>)<sub>2</sub> in THF. Addition of Fe(ClO<sub>4</sub>)<sub>2</sub> from 0 to 13.8 molar equivalents.

#### 4. Cyclic Voltammetric Data

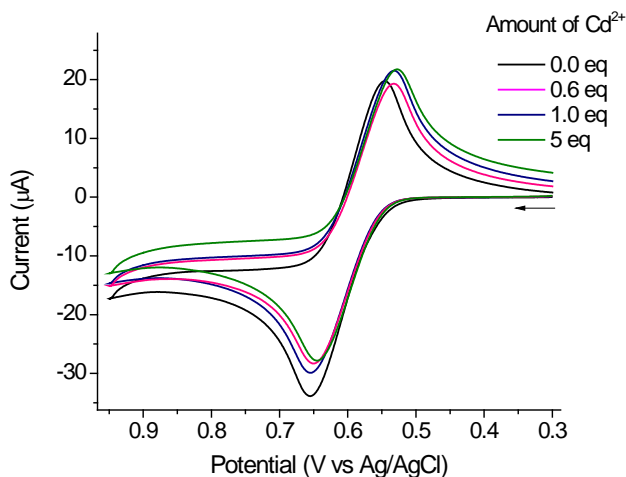


**Fig. S-31.** Cyclic voltammograms of dianthryl TTFV **1** (2.46 mM) in CHCl<sub>3</sub>/acetonitrile (1:3, v/v) upon addition of Cd(ClO<sub>4</sub>)<sub>2</sub>. Electrolyte: Bu<sub>4</sub>NBF<sub>4</sub> (0.1 M), working electrode: glassy carbon, counter electrode: Pt wire, reference electrode: Ag/AgCl, scan rate: 20 mV/s.

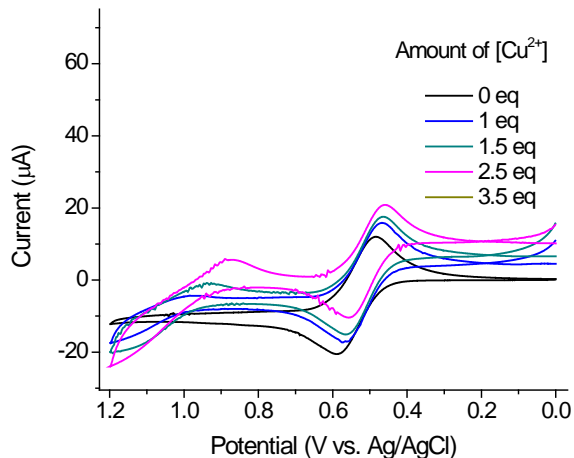


**Fig. S-32.** Cyclic voltammograms of dianthryl TTFV **2** (2.46 mM) in CHCl<sub>3</sub>/acetonitrile (1:3, v/v) upon addition of Cu(OTf)<sub>2</sub>. Electrolyte: Bu<sub>4</sub>NBF<sub>4</sub> (0.1 M), working electrode: glassy carbon, counter electrode: Pt wire, reference electrode: Ag/AgCl, scan rate: 20 mV/s.